Supporting information

Scalable production of bifunctional ordered PtFe alloy electrocatalysts for efficient methanol oxidation and hydrogen evolution

Xuxu Sun, [a,b,‡] Ruiqi Wang, [a,b,‡] Qi Wang, [a,b,c*] Kostya (Ken) Ostrikov [d]

[a] *Institute of Plasma Physics, Hefei Institutes of Physical Science, Chinese Academy of Sciences, Hefei 230031 Anhui, China*

[b] *University of Science and Technology of China, Hefei 230026 Anhui, China*

[c] *College of Chemical Engineering, Sichuan University of Science and Engineering, Zigong 643000, China*

[d] *School of Chemistry and Physics and QUT Centre for Materials Science, Queensland University of Technology (QUT), Brisbane, QLD 4000, Australia*

[‡] These authors contributed equally to this work;

Corresponding Author: Qi Wang, E-mail: qiwang@ipp.ac.cn;

ORCID:

Qi Wang: 0000-0003-3594-2244;

Kostya (Ken) Ostrikov: 0000-0001-8672-9297.

Experimental details

Chemicals: Iron (II) sulfate heptahydrate ($FeSO_4 \cdot 7H_2O$, 99%), chloroplatinic acid hexahydrate ($H_2PtCl_6 \cdot 6H_2O$, 99%), zinc nitrate hexahydrate ($Zn(NO_3)_2.6H_2O$), 2,2'-bipyridine ($C_{10}H_8N_2$, 99%), dopamine hydrochloride ($C_8H_{11}NO_2 \cdot HCl$, 98%), 2-methylimidazole ($C_4H_6N_2$, 98%), absolute ethanol (C_2H_5OH, 99.7%), absolute methanol (CH_3OH, 99.5%) and ammonia ($NH_3 \cdot H_2O$, 25-28%) were purchased from Shanghai Aladdin Biochemical Technology Co., Ltd., China. Sulfuric acid (H_2SO_4, 98%) was purchased from Sinopharm Chemical Reagent Co., Ltd., China. Nafion D520 membrane solution (5 wt%) and commercial JM-20%Pt/C were purchased from Shanghai Hesen Electric Co., Ltd., China. All the chemicals were used as received without any further treatment. Deionized water was obtained from an ultra-pure purification system.

Preparation of the High Nitrogen-Content Carbon (HNC): The HNC powder was prepared according to the previous work with slight modification.[1] Firstly, 14.88 g of Zinc nitrate hexahydrate and 16.22 g of 2-methylimidazole were respectively weighed and dissolved into 400 mL of methanol solution and ultrasonicated for 10 minutes. Then, the 2-methylimidazole solution was quickly poured into the zinc nitrate hexahydrate solution and ultrasonicated them until milky white precipitate appeared. After standing for overnight, the milky white precipitate was cleaned and centrifugated with deionized water and anhydrous ethanol for three times and finally was dried at 60 ℃ for overnight to obtain ZIF-8 precursor powder. After that, 3 g of ZIF-8 precursor powder was weighed and well dispersed into a mixed solution (1000 mL deionized water, 400 mL anhydrous ethanol, and 10 mL ammonia) by sonicating it for 30 minutes. Meanwhile, 500 mg of dopamine hydrochloride was dissolved into a mixed solution (60 mL deionized water and 40 mL anhydrous ethanol) and stirred for 30 minutes. Then, the dopamine hydrochloride mixed solution was poured into the ZIF-8 dispersion and continuously stirred for overnight at room temperature. The brown precipitate was cleaned and centrifuged for three times with deionized water and anhydrous ethanol and finally dried for overnight at 60 ℃ to obtain the ZIF-8@polydopamine precursor powder. After that, the obtained ZIF-8@polydopamine precursor powder was annealed at 900 ℃ in an argon atmosphere for 2 hours and then naturally cooled down to obtain the HNC powder.

Preparation of the PtFe@HNC electrocatalyst: The PtFe compound powder was prepared based on the previous work with slight modification.[2] Specifically, 2 mmol of iron(II) sulfate heptahydrate was

weighed and dissolved into 60 mL of deionized water and stirred for 10 minutes. Meanwhile, 6 mmol of 2,2'-bipyridine (bpy) was weighed and dissolved into 60 mL of anhydrous ethanol and stirred for 10 minutes. Then, the 2,2'-bipyridine ethanol solution was added to the $FeSO_4 \cdot 7H_2O$ solution to form a deep-red complex solution and continuously stirred for overnight. Subsequently, 60 mL of ethanol solution containing 2 mmol $H_2PtCl_6 \cdot 6H_2O$ was gradually added to produce a bright-red precipitate and stirred continuously for more than 5 hours. After that, the bright-red PtFe compound precipitate was cleaned and centrifuged with ethanol solution for several times and dried at 60 ℃ for overnight. The obtained PtFe complex precursor powder (800 mg) and HNC powder (800 mg) were respectively dispersed in 200 mL of ethanol solution, followed by ultrasonic treatment and magnetic stirring for 2 hours to make them relatively more dispersed. Then, the powder dispersions were thoroughly stirred and mixed by ultrasonic stirring and finally dried at 60 ℃ for overnight to obtain the black-red PtFe compound/HNC composite powder. Ultimately, the prepared PtFe compound/HNC composite precursor powder was annealed at 700 ℃ under Ar atmosphere for 6 hours to obtain an ordered PtFe alloy/high nitrogen-content carbon composite electrocatalyst, named as PtFe@HNC.

Materials Characterization: The samples' morphology, mean nanoparticle size and crystal plane structure were respectively observed through scanning electron microscopy (SEM, SIRION200, 3 kV) and transmission electron microscopy (TEM, JEM-2100F, 200 kV). The high-angle annular dark-field scanning transmission electron microscopy (HAADF-STEM) and energy dispersive spectroscopy (EDS) mapping images were obtained using high-resolution transmission electron microscopy (HRTEM, FEI Talos F200X, 200 kV). The X-ray diffraction (XRD) image was performed on a X'Pert through the graphite monochromatized Cu-Kα radiation (λ=1.54178Å) from 20° to 80°. The Brunauer–Emmett–Teller (BET) surface area, and relative pore size distribution analysis were done on a Tristar II 3020M. The X-ray photoelectron spectroscopy (XPS) was measured on a Thermo ESCALAB 250Xi with the Al Kα =1486.6 eV. The metal loading was obtained from Inductively coupled plasma atomic emission spectroscopy (ICP-AES, Optima 7300 DV) equipment.

***Electrochemical Measurements*:** All electrochemical tests were completed on the electrochemical workstation (CHI 660E) with standard three-electrode system using Ag/AgCl (3 M KCl) as the reference electrode, glassy carbon electrode (GCE, diameter 3 mm) as the working electrode, and platinum wire as the counter electrode. The catalyst slurry was obtained by adding 2 mg as-prepared sample into the mixture solution of 500 μl deionized water, 500 μl absolute ethanol and 30 μl Nafion

(D520, 5 wt%) and ultrasonicated for 60 minutes. Then, 5 μl of the catalyst ink (2 mg/ml, 14.5 wt% Pt loading measured by ICP-AES) was dripped onto a pre-cleaned GCE and naturally dried to form a uniform film. All electrochemical measurements were conducted in N_2-saturated sulfuric acid medium.

For methanol oxidation reaction (MOR) testing, the working electrode was activated in 0.5 M H_2SO_4 aqueous solution through cycling potential between -0.2 and 1.0 V vs. Ag/AgCl for 50 cycles at 50 $mV \cdot s^{-1}$ for the calculation of electrochemical specific aera (ECSA) using the following equation[3]: $ECSA = Q_H/(M_{Pt}*0.21\ mC/cm^2)$, where Q_H is the charge of H_{upd} adsorption, M_{Pt} is the loading amount of Pt, 0.21 mC/cm^2 is the charge of oxidizing monolayer of H_2 absorption on the surface. And then, CV curves were operated between 0 and 1.0 V vs. Ag/AgCl in 0.5 M H_2SO_4 + 1 M CH_3OH aqueous solution to determine the electrocatalysts' activity for MOR. To make the tests more rigorous, the loading content of Pt was determined as 14.5 wt% by ICP-AES. CA curves (4000 s, at 0.60 V vs. Ag/AgCl) and CV curves (1000 cycles, at 200 mV/s) were performed in 0.5 M H_2SO_4 containing 1M CH_3OH to check the durability of electrocatalysts.

For hydrogen evolution reaction (HER) testing, all potentials were transformed to RHE with the following equation[4]: $E\ (RHE) = E\ (Ag/AgCl) + 0.226\ V$. Firstly, the working electrode was activated in 0.5 M H_2SO_4 solution through the potential cycling between 0.1 and -0.4 V vs. RHE at 50 mV/s until stable voltammogram curves were obtained. The electrocatalytic performance of HER was acquired by linear sweep voltammograms (LSV) at 5 mV/s and all polarization curves were corrected with iR compensation for 90%. The Tafel slope (b) was calculated with the following equation: $\eta = a + b\ log\ (j)$, where η is the overpotential (mV) and j is the current density (mA/cm^2). Turnover frequency (TOF) values were obtained by the following equation: $TOF\ (s^{-1}) = I/(2*F*n)$, where I is the current (mA) during the LSV testing, F is the Faraday's constant (96485 C/mol), n is the number of active sites (mol). Electrochemical impedance spectroscopy (EIS) spectra were recorded ranging from 100 kHz to 10 mHz with the amplitude of 10 mV. CV curves were operated by cycling potential between 0.1 and -0.4 V vs. RHE at 200 mV/s to evaluate the catalytic stability of catalysts for HER. Chronopotentiometric (CP) curve was performed at 10 mA/cm^2 to further verify the superior durability of PtFe@HNC electrocatalyst for HER.

Results

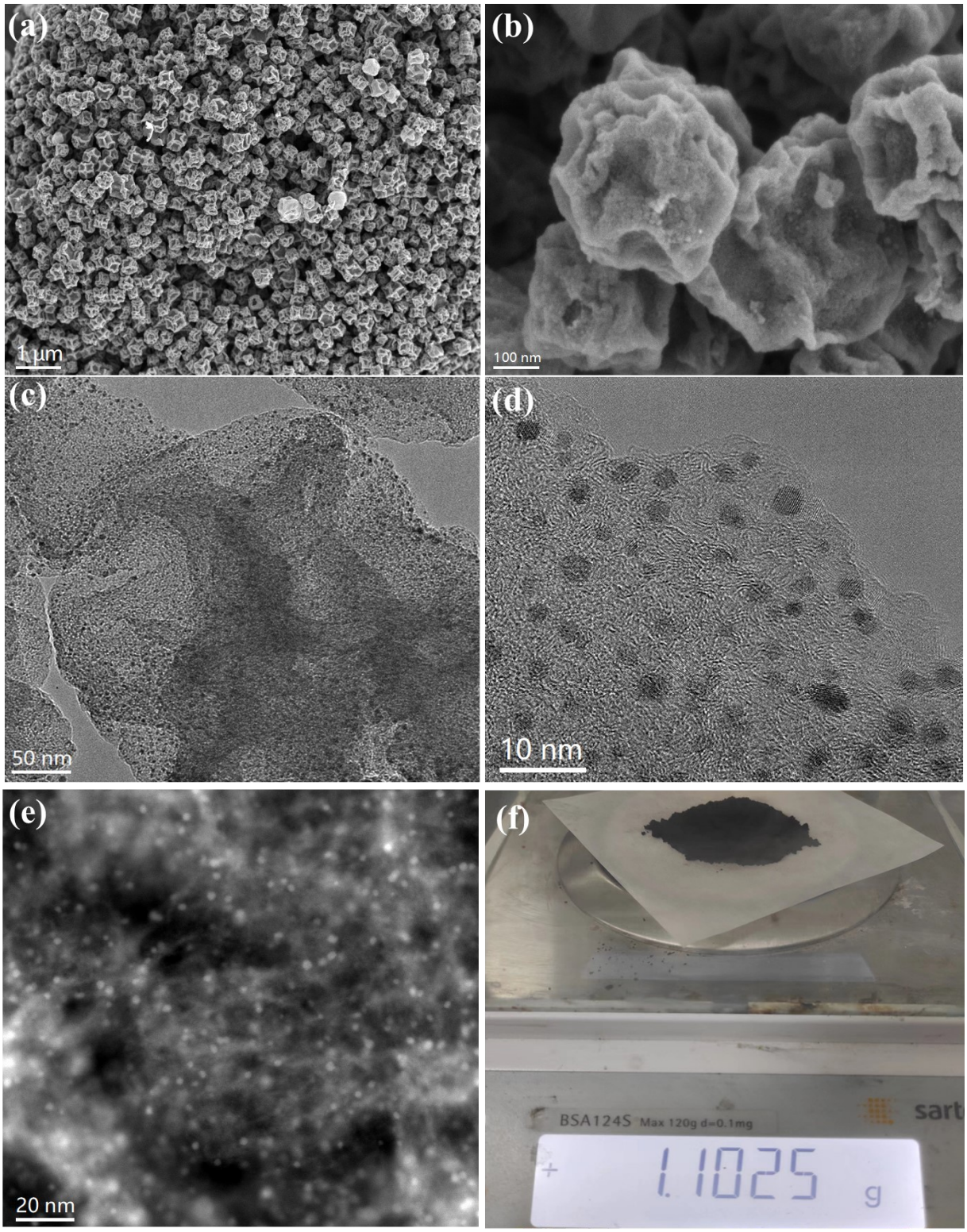

Figure S1. Physical characterization of the PtFe@HNC electrocatalyst. (a) and (b) SEM images. (c) and (d) TEM images. (e) HAADF-STEM image. (f) Electronic photo for the gram-scale synthesis of PtFe@HNC electrocatalyst.

Table S1. Lattice strain and ordering degree of PtFe@HNC.*

Sample	2θ(degree) (111)	Lattice spacing d (Å)	Lattice constrain (%)	Ordering degree (%)
Pt-PDF# (04-0802)	39.76	2.27	--	--
PtFe@HNC	40.86	2.25	-0.88	79.25

* According to the parameters from XRD and HRTEM with the following equation:

Lattice strain $\varepsilon = \frac{d_{Pt-Fe} - d_{Pt-Pt}}{d_{Pt-Pt}} * 100\%$

The ordering degree of PtFe@HNC was calculated through the following equation (2):

Ordering degree $l = \frac{S_{(110)}}{S_{(111)} + S_{(200)} + S_{(002)}} * 100\%$

Where the $S_{(110)}$, $S_{(111)}$, $S_{(200)}$, $S_{(002)}$ respectively refers to the aera of XRD powder diffraction peaks (110), (111), (200) and (002).And the standard value of ordering degree for *fct*-PtFe was 0.1843, which can be normalized to 100% ordering intermetallic PtFe.[2]

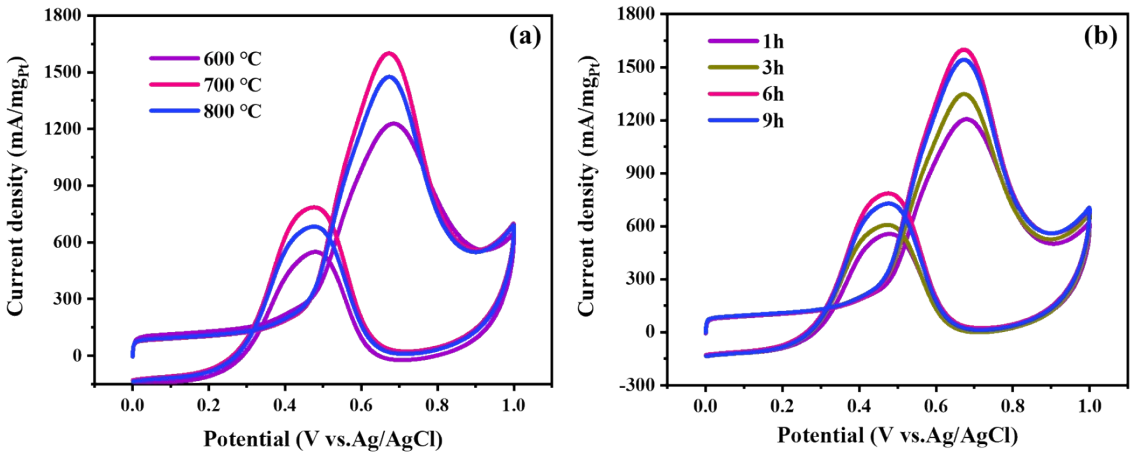

Figure S2. CV curves of PtFe@HNC with different annealing temperature (a) and time (b) in N_2-saturated 0.5 M H_2SO_4 + 1 M CH_3OH solution.

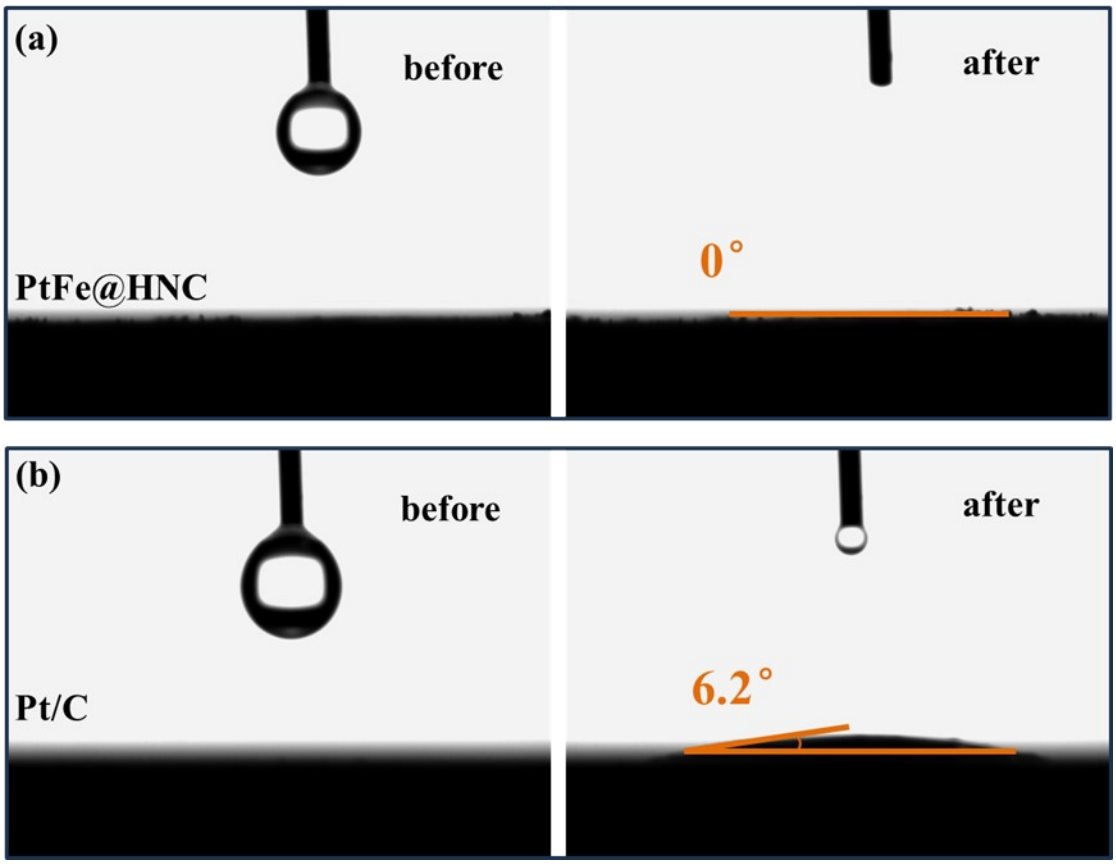

Figure S3. Contact angles of 0.5 M H_2SO_4 solution with (a) PtFe@HNC and (b) Pt/C electrodes.

Table S2. Electrocatalytic activity of PtFe@HNC and commercial Pt/C toward MOR

Samples	ECSA (m^2/g)	E_{onset} (V)	I_f (mA/mg_{Pt})	I_f/I_b
PtFe@HNC	49.6	0.30	1599.3	2.04
Pt/C	56.8	0.41	299.1	0.82

Table S3. Summary of recently reported Pt-based electrocatalysts toward MOR.

Samples	Electrolyte	Mass activity（mA/mg）	Specific activity（mA/cm²）	Ref.
PtFe@HNC	0.5 M H_2SO_4+ 1 M CH_3OH	1599.3	3.22	This work
PtFe@a-FeO_x/NC-C	0.5 M H_2SO_4+ 1 M CH_3OH	1480	2.34	5
Pt-SnO_2-rGO	0.1 M $HClO_4$+ 1 M CH_3OH	1310	2.18	6

PtFeAu NCs	0.5 M H_2SO_4+ 1 M CH_3OH	1324	3.01	7
PtFe/C@NC-3	0.5 M H_2SO_4+ 1 M CH_3OH	357.9	0.84	8
PtRuFe nanodendrites	0.5 M H_2SO_4+ 1 M CH_3OH	1140	2.03	9
PtFe@PtRuFe	0.1 M $HClO_4$+ 1 M CH_3OH	690	1.3	10
Pt-Ni_2P-Graphene	0.5 M H_2SO_4+ 1 M CH_3OH	1554.6	1.64	11
PtIrCu-NCs	0.1 M $HClO_4$+ 1 M CH_3OH	863	1.04	12
PtCoNiRh NWs	0.1 M $HClO_4$+ 1 M CH_3OH	1360	2.08	13
PtNiP/P-graphene	0.5 M H_2SO_4+ 1 M CH_3OH	826.1	0.65	14

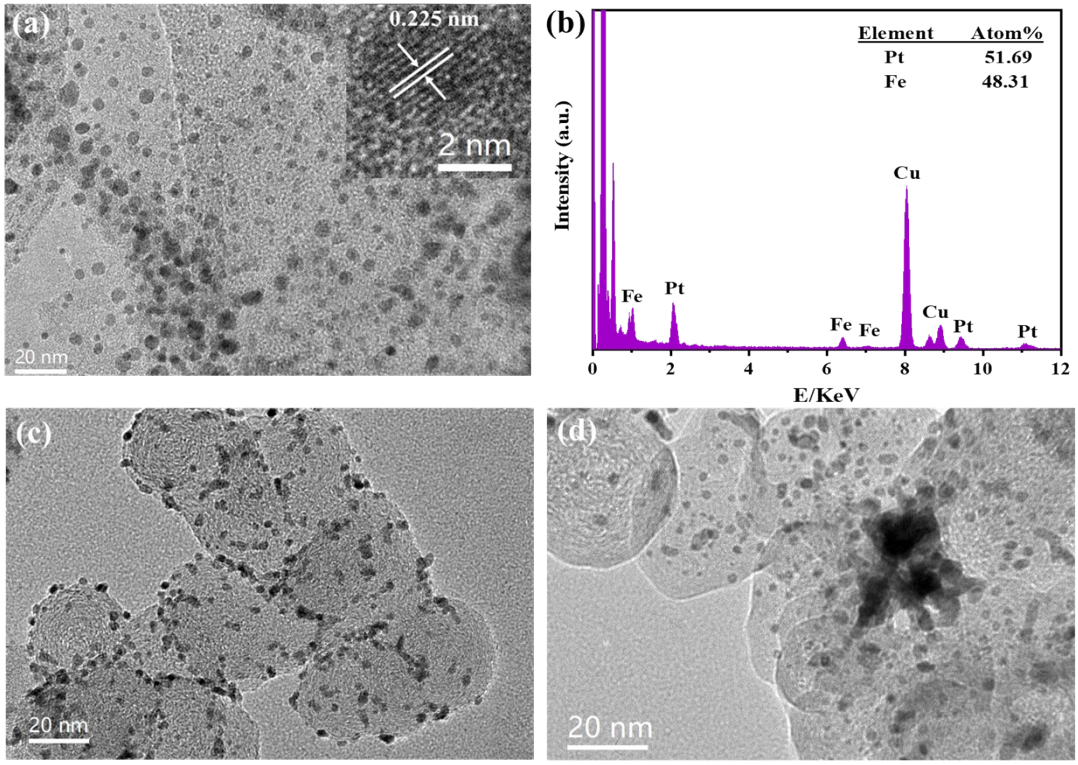

Figure S4. (a) and (b) TEM and STEM-EDS images of PtFe@HNC after 4000 s chronoamperometric measurement toward MOR, the inset is HRTEM for interplanar spacing. (c) and (d) TEM images of commercial Pt/C before and after 4000s chronoamperometric measurement toward MOR.

$$CH_3OH + * \rightarrow CH_2OH^* + H^+ + e^- \quad (1)$$

$$CH_2OH^* \rightarrow CHOH^* + H^+ + e^- \quad (2)$$

$$CHOH^* \rightarrow COH^* + H^+ + e^- \quad (3)$$

$$COH^* \rightarrow CO^* + H^+ + e^- \quad (4)$$

$$CO^* + H_2O \rightarrow CO^* + OH^* + H^+ + e^- \quad (5)$$

$$CO^* + OH^* \rightarrow CO_2 + H_2O + H^+ + e^- \quad (6)$$

Figure S5. The involved multiple-electrons transfer routes for MOR.

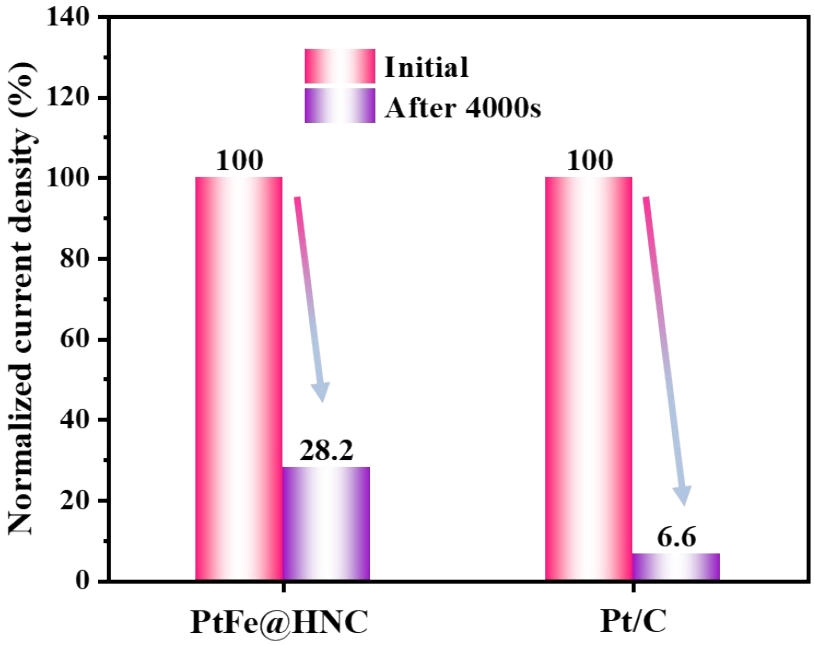

Figure S6. Retention of mass activity for PtFe@HNC and commercial Pt/C after 4000 s chronoamperometric measurement in N_2-saturated 0.5 M H_2SO_4 and 1 M CH_3OH solution.

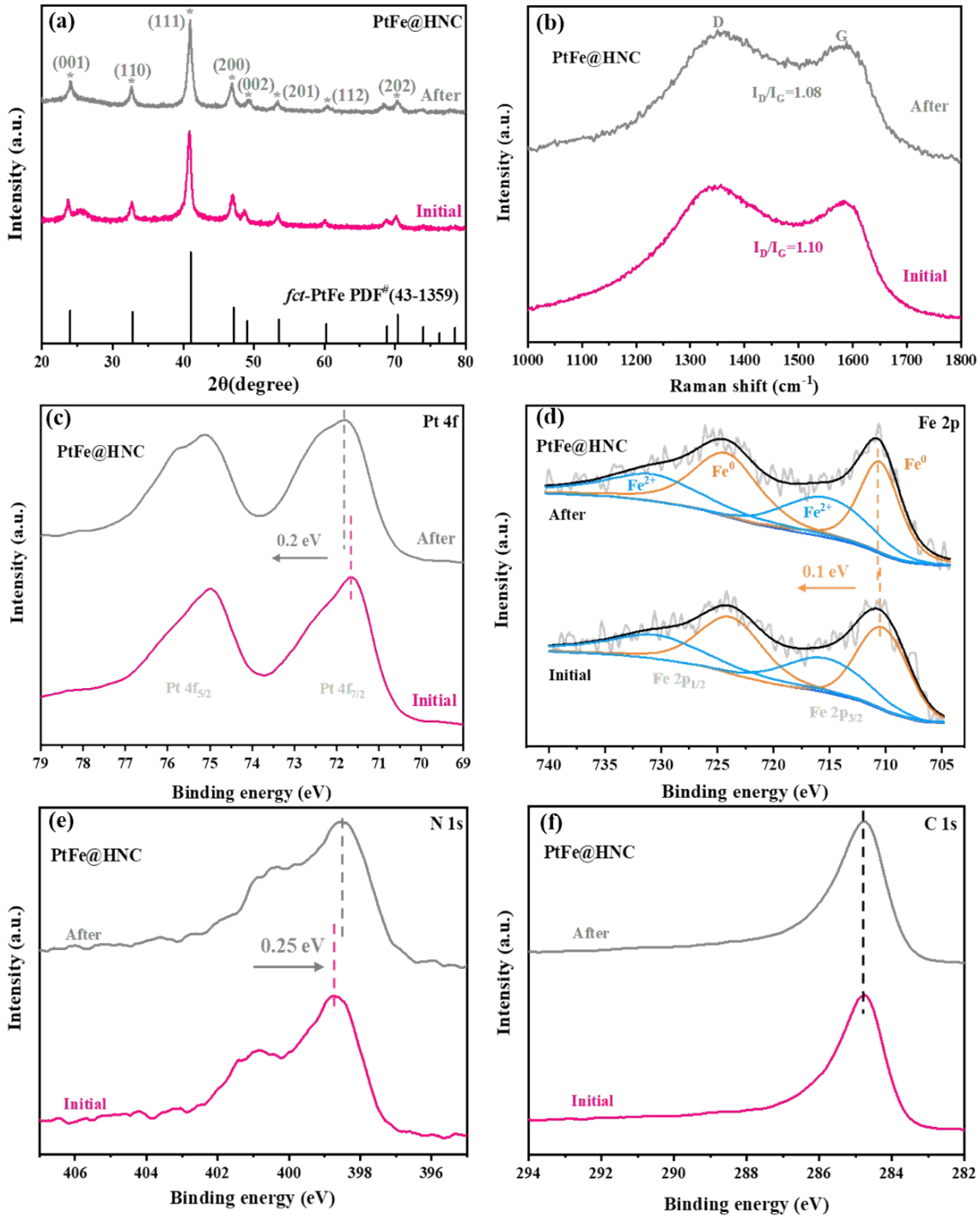

Figure S7. Crystalline structures, vibrational modes and elemental bonding states of the PtFe@HNC electrocatalyst before and after 4000 s chronoamperometric MOR testing. (a) XRD patterns. (b) Raman spectra. (c) Pt 4f XPS spectra. (d) Fe 2p XPS spectra. (e) N1s XPS spectra. (f) C1s XPS spectra.

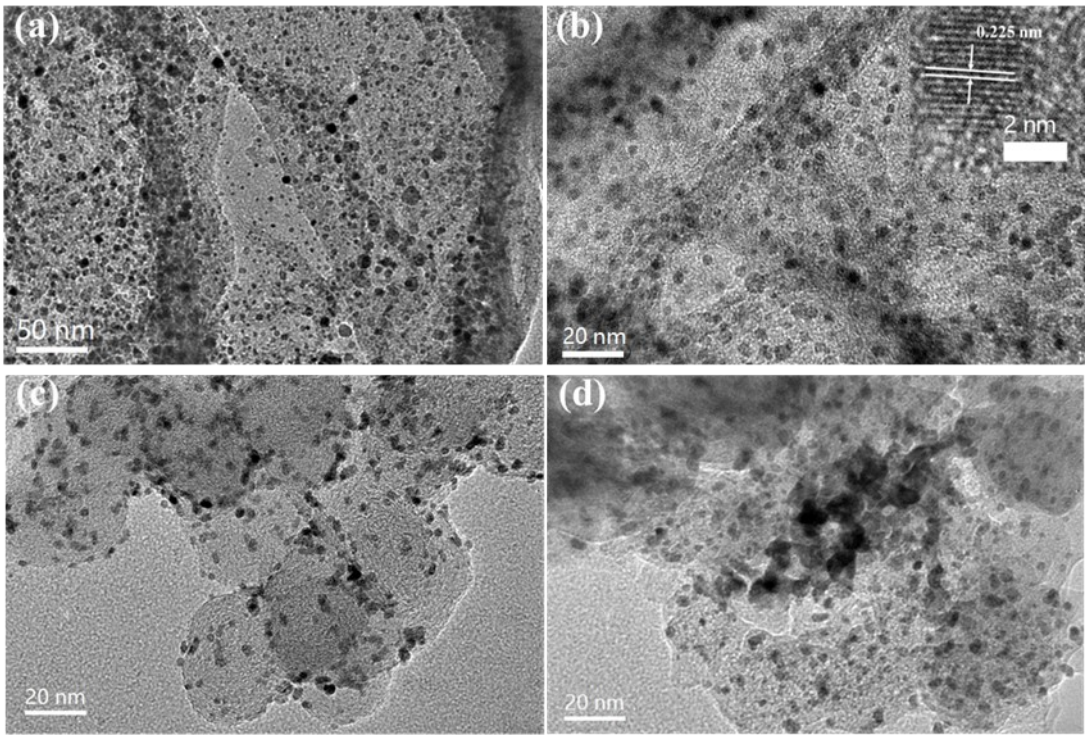

Figure S8. (a) and (b) TEM images of PtFe@HNC after accelerated 5000 sweeps toward HER, the inset is HRTEM for interplanar spacing. (c) and (d) TEM images of commercial Pt/C before and after accelerated 5000 sweeps toward HER.

Table S4. Summary of recently reported Pt-based electrocatalysts toward HER.

Samples	Electrolyte	Overpotential (mV)	Tafel slop（mV/dec）	Ref.
PtFe@HNC	0.5 M H_2SO_4	15	12.5	This work
Pt/NiCo@C	0.5 M H_2SO_4	17	32	15
Pt/TiO_2-O_v	0.5 M H_2SO_4	18	12	16
Pt_5/HMCS	0.5 M H_2SO_4	20.7	28.3	4
Pt NPs/Siloxene	0.5 M H_2SO_4	24	24.6	17
$Pt_{0.47}$-Ru/Acet	0.5 M H_2SO_4	28	33.3	18
Pt-Ni NPs	0.5 M H_2SO_4	32	51	19

Pt/Mxene	0.5 M H_2SO_4	34	29.7	20
ALD50Pt/NGNs	0.5 M H_2SO_4	40	29	21
Pt-NCs-Mxene	0.5 M H_2SO_4	40	51	22
Pt SA/m-WO_{3-x}	0.5 M H_2SO_4	45	47	23
CuTi@Pt	0.5 M H_2SO_4	46	33.3	24

References

1 R. Yun, T. Li, B. Zhang, et al., Amino induced high-loading atomically dispersed Co sites on N-doped hollow carbon for efficient CO_2 transformation, *Chemical Communications*, 2022, **58**, 6602-6605.

2 C. Yang, L. Wang, P. Yin, et al., Sulfur-anchoring synthesis of platinum intermetallic nanoparticle catalysts for fuel cells, *Science*, 2021, **374**, 459-464.

3 J. Yang, R. Hubner, J. Zhang, et al., A robust PtNi nanoframe/N-doped graphene aerogel electrocatalyst with both high activity and stability, *Angew. Chem., Int. Ed.*, 2021, **60**, 9590-9597.

4 X. Wan, H. Wu, B. Guan, et al., Confining Sub-nanometer Pt clusters in hollow mesoporous carbon spheres for boosting hydrogen evolution activity, *Advanced Materials*, 2020, **32**, e1901349.

5 W. Zhao, L. Ma, M. Gan, et al., Engineering intermetallic-metal oxide interface with low platinum loading for efficient methanol electrooxidation, *Journal of Colloid and Interface Science*, 2021, **604**, 52-60.

6 Y. W. Zhou, Y. F. Chen, K. Jiang, et al., Probing the enhanced methanol electrooxidation mechanism on platinum-metal oxide catalyst, *Applied Catalysis B: Environmental*, 2021, **280**, 119393.

7 Z. Cai, Z. Lu, Y. Bi, et al., Superior anti-CO poisoning capability: Au-decorated PtFe nanocatalysts for high-performance methanol oxidation, *Chemical Communications*, 2016, **52**, 3903-3906.

8 Y. Nie, X. Qi, R. Wu, et al., Structurally ordered PtFe intermetallic nanocatalysts toward efficient electrocatalysis of methanol oxidation, *Applied Surface Science*, 2021, **569**, 151004.

9 Z. Cai, Y. Kuang, X. Qi, et al., Ultrathin branched PtFe and PtRuFe nanodendrites with enhanced electrocatalytic activity, *Journal of Materials Chemistry A*, 2021, **3**, 1182-1187.

10 Q. Wang, S. Chen, P. Li, et al., Surface Ru enriched structurally ordered intermetallic PtFe@PtRuFe core-shell nanostructure boosts methanol oxidation reaction catalysis, *Applied Catalysis B: Environmental*, 2019, **252**, 120-127.

11 H. Liu, D. Yang Y. Bao, et al., One-step efficiently coupling ultrafine Pt–Ni_2P nanoparticles as robust catalysts for methanol and ethanol electro-oxidation in fuel cells reaction, *Journal of Power Sources*, 2019, **434**, 226754.

12 Y. H. Ahmad, H. A. El-Sayed, A. T. Mohamed, et al., Rational one-pot synthesis of ternary PtIrCu nanocrystals as robust electrocatalyst for methanol oxidation reaction, *Applied Surface Science*, 2020, **534**, 147617.

13 W. Wang, X. Chen, X. Zhang, et al., Quatermetallic Pt-based ultrathin nanowires intensified by Rh enable highly active and robust electrocatalysts for methanol oxidation, *Nano Energy*, 2020, **71**, 104623.

14 L. Yang, G. Li, R. Ma, et al., Nanocluster PtNiP supported on graphene as an efficient electrocatalyst for methanol oxidation reaction, *Nano Research*, 2021, **214**, 853-2860.

15 G. Jiang, C. Zhang, X. Liu, et al., Electrocatalytic hydrogen evolution of highly dispersed Pt/NC nanoparticles derived from porphyrin MOFs under acidic and alkaline medium, *International Journal of Hydrogen Energy*, 2022, **47**, 6631.

16 Z. Wu, P. Yang, Q. Li, et al., Microwave synthesis of Pt clusters on black $TiO_{(2)}$ with abundant oxygen vacancies for efficient acidic electrocatalytic hydrogen evolution, *Angew. Chem. Int. Ed.*, 2023, **62**, e202300406.

17 Q. Chen, C. Du, Y. Yang, Q. Shen, J. Qin, M. Hong, X. Zhang, J. Chen, Two-dimensional siloxene as an advanced support of platinum for superior hydrogen evolution and methanol oxidation electrocatalysis, *Materials Today Physics*, 2023, **30**, 100931.

18 Y. Chen, J. Li, N. Wang, Y. Zhou, J. Zheng, W. Chu, Plasma-assisted highly dispersed Pt single atoms on Ru nanoclusters electrocatalyst for pH-universal hydrogen evolution, *Chemical Engineering Journal*, 2022, **448**, 137611.

19 H. Zhai, G. Xu, J. Liu, T. Xu, C. Li, J. Bai, Boosting activity and stability by coupling Pt–Ni nanoparticles with La-modified flexible carbon nanofibers for hydrogen evolution reaction, *International Journal of Hydrogen Energy*, 2022, **47**, 2423.

20 Y. Wu, W. Wei, R. Yu, L. Xia, et al., Anchoring sub-nanometer Pt clusters on crumpled paper-like MXene enables high hydrogen evolution mass activity, *Advanced Functional Materials*, 2022, **32**, 2110910.

21 N. Cheng, S. Stambula, D. Wang, et al., Platinum single-atom and cluster catalysis of the hydrogen evolution reaction, *Nat. Commun.*, 2016, **7**, 13638.

22 X. Jian, T. T. Wei, M. M. Zhang, R. Li, J. X. Liu, Z. H. Liang, Construction of $Ti_3C_2T_x$ MXene supported low-platinum electrocatalyst for hydrogen evolution reaction by direct electrochemical strategy, *Journal of the Electrochemical Society*, 2021, **168**, 096504.

23 J. Park, S. Lee, H. E. Kim, et al., Investigation of the support effect in atomically dispersed Pt on $WO_{(3-x)}$ for wtilization of Pt in the hydrogen evolution reaction, *Angew. Chem. In.t Ed.*, 2019, **58**, 16038.

24 T. Chuyen Phan, V. T. Nguyen, H. S. Choi, H. Kim, Highly efficient and durable electrochemical hydrogen evolution reaction based on composition/shape controlled CuTi@Pt core-shell nanotubes in acidic media, *Applied Surface Science*, 2022, **605**, 154331.